RSC Advances

PAPER

View Article Online
View Journal | View Issue

Cite this: *RSC Adv.*, 2017, **7**, 13979

Distribution of oxygen functional groups of graphene oxide obtained from low-temperature atomic layer deposition of titanium oxide†

Dong Seok Shin,‡[a] Hyun Gu Kim,‡[b] Ho Seon Ahn,‡[c] Hu Young Jeong,[d] Youn-Jung Kim,[e] Dorj Odkhuu,[a] N. Tsogbadrakh,[f] Han-Bo-Ram Lee*[b] and Byung Hoon Kim*[a]

Received 4th January 2017
Accepted 21st February 2017

DOI: 10.1039/c7ra00114b

rsc.li/rsc-advances

The distribution of oxygen functional groups on the surface of graphene oxide (GO) has been investigated experimentally and theoretically. Atomic layer deposition of TiO_x was used to clarify the location of oxygen functional groups. We found that the oxygen functional groups are distributed in the form of islands, which is confirmed using aberration corrected transmission electron microscopy and X-ray photoelectron spectroscopy. The density functional studies further support these findings. The evolution of oxygen functional groups was also investigated with GO treated at 150, 200, 250, and 300 °C. In addition, the reduction of epoxide and hydroxyl groups on the GO surface at different temperatures has been discussed in connection with ab initio molecular dynamics simulations.

Introduction

Graphene oxide (GO) had been revisited due to the possibility of the mass production of graphene.[1] GO has attracted lots of attention as a building block for novel applications towards not only enhancement of electrochemical performance,[2–7] gas storage capacity,[8–11] and efficiency of solar cells[12] but also development of artificial muscle[13] and shape-memory polymers,[14] and so on. Even though the existence of functional groups and large surface area have been suggested as the dominant factors for these superior properties of GO in the various fields, the exact mechanisms are still veiled. Hence, the structure of GO must be verified to understand the reason for the outstanding properties and to improve the efficiency in energy storage, gas sensing properties, and other applications. Especially, the distribution of the oxygen functional groups is the most important to understand the mechanisms,[15,16] for example, the pathway of Li ions and charge storage in a GO-based Li-ion battery and supercapacitor, respectively. The existence of functional groups such as epoxy, hydroxyl, and carboxyl surface groups[17,18] was already known, and the quantity of the functional groups with respect to a graphitic region have been reported experimentally[19,20] and theoretically.[21] Moreover, the atomic structure of a highly-reduced GO (rGO) using chemical agents and high temperature over 550 °C (ref. 22–24) has been established. However, the structure of GO at low temperature is more important to understand the energy storage of GO[8,25] and pillared GO.[10] Nevertheless, the distribution of the oxygen functional groups in GO at low temperature has rarely been investigated[26,27] because the functional groups in a wide region of GO surface cannot be identified clearly.

Herein, we report the results of experimental and theoretical investigations on the distribution of oxygen functional groups over GO surface. The experiments were performed using a titanium nanostructure deposited on the oxygen groups of GO by atomic deposition layer (ALD) method. Since a thin film by ALD forms only through surface reactions of precursors with surface species, the nucleation of ALD film strongly depends on the surface species. Surface reaction mechanisms of TiO_2 ALD has been many times reported through experimental and theoretical studies, and it has been known that Ti precursor chemisorbs on surface *via* reactions with oxygen species, such as $(OH)_x^*$ and O_x.[28–30] The pristine graphene surface is chemically inert, so that the Ti precursor is hard to adsorb on the surface for initiating nucleation of TiO_2. Therefore, once nuclei of ALD TiO_2 are formed on graphene surface, it can be inferred that the graphene surface has reactive oxygen functional groups, which

[a]Department of Physics, Incheon National University, Incheon 22012, Republic of Korea. E-mail: kbh37@inu.ac.kr
[b]Department of Materials Science and Engineering, and Innovation Center for Chemical Engineering, Incheon National University, Incheon 22012, Republic of Korea. E-mail: hbrlee@inu.ac.kr
[c]Department of Mechanical Engineering, Incheon National University, Incheon 22012, Republic of Korea
[d]UNIST Central Research Facilities (UCRF), School of Materials Science and Engineering, UNIST, Ulsan 44919, Republic of Korea
[e]Department of Marine Science, Incheon National University, Incheon 22012, Republic of Korea
[f]Department of Physics, National University of Mongolia, Ulaanbaatar 14201, Mongolia

† Electronic supplementary information (ESI) available. See DOI: 10.1039/c7ra00114b

‡ These author contributed equally to this work.

promote Ti precursor adsorptions, such as $(OH)_x^*$ and O_x. In other words, the oxygen functional groups can be traced through analyze of ALD TiO_2 formation on graphene. Titanium oxide was deposited at various temperatures (150, 200, 250, and 300 °C) using low temperature deposition method. The distribution was observed and compared with aberration corrected transmission electron microscopy (TEM), which shows that the oxygens are distributed with the form of island. This was further confirmed by X-ray photoelectron spectroscopy (XPS) and density functional theory (DFT) studies. Moreover, the experimentally observed reduction process of epoxide and hydroxyl groups on GO surface at the elevated temperature has been discussed in connection with ab initio molecular dynamic (AIMD) simulations.

Experimental

We prepared the titanium oxide-deposited GO (TiGO) using ALD. The procedure is as follows. GO was synthesized by a modified Hummers method with graphite powder of 450 nm size. The graphite was oxidized with concentrated H_2SO_4, $K_2S_2O_8$ and P_2O_5. After filtering, washing, and drying the product was re-suspended in concentrated H_2SO_4 and oxidized further with $KMnO_4$ and H_2O_2; the result was a thick, brownish yellow GO suspension. The GO suspension was centrifuged and washed with 10% HCl and DI water, and then the suspension was dried at 50 °C for three days to obtain GO. The well dispersed GO in DI water was dropped on Mo TEM grid. Prior to ALD process, the Mo TEM grid was annealed at 150, 200, 250, and 300 °C for 20 minutes to reduce GO in the ALD chamber. Hence, ALD of titanium oxide was performed on rGO in a commercial ALD system (SN-100, SNTEK) using titanium(IV) isopropoxide 97% (TTIP) precursor (Sigma-Aldrich) and H_2O reactant. The ALD system is a traveling wave type chamber and capable up to 4 inch wafer and further detail configuration of ALD chamber can be found in our previous paper.[31] N_2 was used for purging gas. Substrate temperature was controlled from 150 to 300 °C, and the bubbler was heated at 50 °C to obtain a proper vapour pressure. Both exposure times of TTIP precursor and H_2O reactant were 2 s, and purging times after precursor exposure and reactant exposure were 15 s and 30 s, respectively. The thickness of the deposited titanium oxide thin film was fixed to 1.0 nm by changing the number of ALD cycle number. TEM study was performed by aberration corrected TEM (FEI Titan cube G2 60-300) operated at an accelerating voltage of 80 kV. XPS of the samples was measured with PHI 5000 Versa Probe II (ULVAC-PHI) using a monochromatic Al-Kα X-ray source at 23.1 W.

Computation method

The DFT simulations were carried out within the framework of the projector augmented-wave formalism[32] as implemented in the Vienna ab initio simulation package (VASP).[33] The generalized gradient approximation formulated by Perdew, Burke, and Ernzerhof was employed for the exchange correlation potential.[34] We used an energy cutoff of 400 eV and a *k*-point sampling of 3 × 3 × 1 for the 6 × 6 graphene cell with periodic boundary conditions along the *xy*-direction. The vertical vacuum size of the supercell along the *z*-axis was chosen no less than 15 Å to avoid a possible interaction between the repeated layers (an isolated graphene). We optimize the in-plane lattice for each sample while kept fixed the *z*-axis. The optimization of both lattice and atomic positions proceeds until the changes in energy were less than 10^{-5} eV per cell and the forces acting on atoms were less than 10^{-2} eV $Å^{-1}$. Both the spin-polarized and spin-non-polarized calculations were taken into account (Table S1 in the ESI†), and results presented in the following paragraphs are those from the spin-polarized calculations. In the AIMD simulations, we use a time step of 2 fs and a Nose thermostat[35] to model a canonical ensemble. A total simulation time was thus 2 ps and there is no difference between temperature profiles at 2 and 4 ps. All the AIMD calculations were performed at the constant volume and same evaluated simulation temperature, where a *k*-point sampling and energy cutoff were restricted to the *Γ* point and 300 eV, respectively.

Results and discussion

The deposition of titanium oxide on graphene oxide was confirmed by XPS study. Fig. 1 shows the O 1s spectra of TiGO as a function of the deposition temperature. The O═C–OH at 530.80 eV, C═O at 531.75 eV, and C–OH at 532.99 eV were observed in the pristine GO. After ALD process, the peak corresponding to the titanium oxide at 529.15 eV was developed. This peak increased with the increase of the deposition temperature. Since the detachment of oxygen functional groups from GO layers becomes enhanced as the temperature increases, the quantity of titanium oxide (red arrow in Fig. 1) increases with respect to that of oxygen functional groups. Titanium oxide deposition onto GO surface was also proved by TEM.

The single-layer GO was used to investigate the oxygen distribution (inset of Fig. 2a). Titanium oxide-deposited GO at 150 °C (TiGO150, the number 150 indicates the deposition temperature) is shown in Fig. 2. The three representative structures were observed; the clean hexagonal region, nanocrystalline structures, and bright amorphous structure. The clean hexagonal regions are graphitic carbons without any oxygen functional groups (sp^2

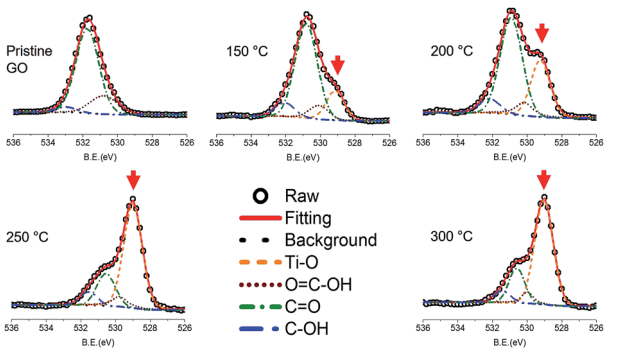

Fig. 1 O 1s XPS spectra of TiGO as a function of the deposition temperature. The red arrow indicates the peak corresponding to titanium oxide.

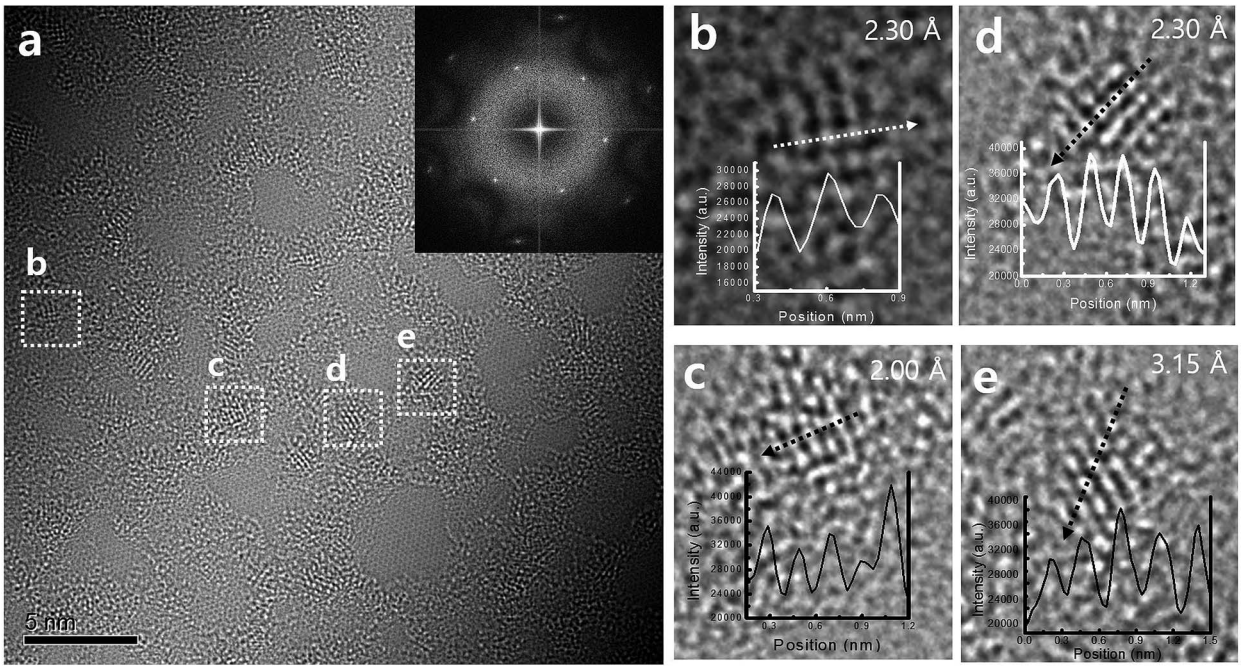

Fig. 2 TEM images of (a) TiGO150 and (b–e) the profiles of nanocrystalline structure. The lattice spacings are (b) 2.30 Å, (c) 2.00 Å, (d) 2.30 Å, and (e) 3.15 Å, which correspond to the structure of rutile TiO_2.

carbon). Nanocrystalline structures with 1–2 nm of size were not distributed evenly. Although they were identified as TiO, TiO_2, and Ti_2O_3, we found that the rutile TiO_2 was the main nanostructure among them, which was proved by the profiles of the magnified TEM images (Fig. 2b–e). We observed the lattice spacings of d = 2.30, 2.00, and 3.15, which respectively correspond to the lattice spacings for (220), (210), and (110) planes of the rutile TiO_2. In the case of the bright amorphous atoms, although we cannot define them at this stage, they are to be the noncrystalline titanium oxide.

It is well established that the oxygen functional groups are desorbed at high temperature and this behaviour is enhanced with the increase of temperature. This was also confirmed using the variation of C 1s peak in XPS study (Fig. 3). The C=C bond at 283.85 eV, C–OH bond at 284.58 eV, C–O–C bond at 285.99 eV, C=O bond at 286.89 eV, and O=C–O bond at 287.39 eV were found in the pristine GO. The C=C bonds increased from 40.470% for pristine GO to 80.012% for TiGO300. On the contrary, the oxygen functional groups, C–OH, C–O–C, C=O, and O=C–O, decreased as the deposition temperature increased. TEM study also shows this behaviour (Fig. 4). Although the clean hexagonal region (bright grey in Fig. 4), *i.e.*, the area for sp^2 carbons did not increase up to 80% of total

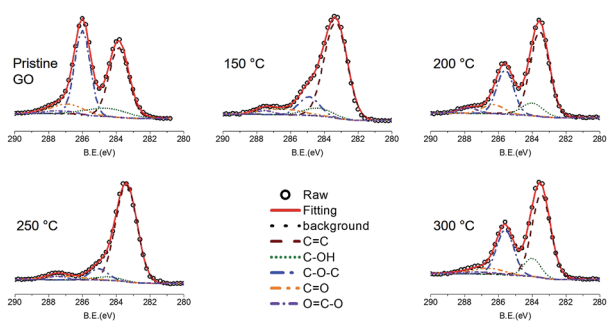

Fig. 3 C 1s XPS spectra of TiGO as a function of the deposition temperature. The oxygen functional groups decreased as the temperature increased.

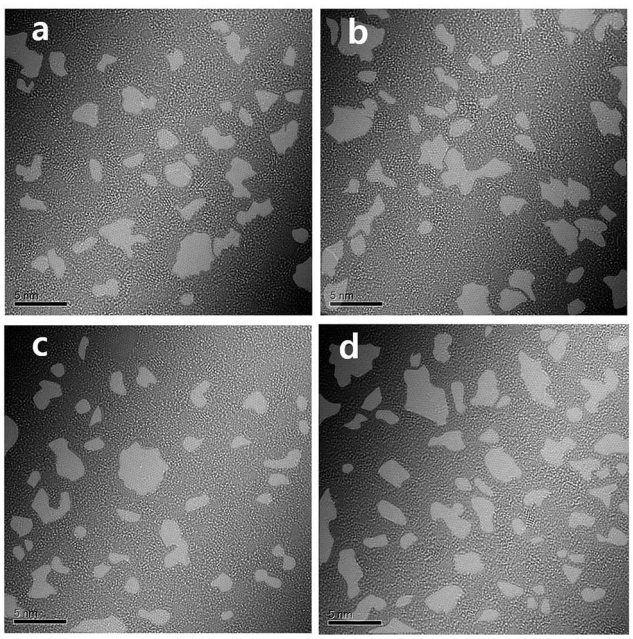

Fig. 4 TEM image of TiGO treated at various deposition temperatures (a) 150 °C, (b) 200 °C, (c) 250 °C, (d) 300 °C. The grey colour indicates the clean hexagonal region.

region in TEM image of TiGO300, we found that it became larger as the deposition temperature increased (from 19.2% for TiGO150 to 29.9% for TiGO300). Note that the titanium oxide and amorphous bright regions are not evenly distributed. They are gathered in the form of the islands which are distributed irregularly.

To better certify the aforementioned results, we conduct the first-principles DFT and AIMD calculations. We first explore the structural features and energetics of oxidation functional groups on a single-layer graphene. The modelled geometries consist of the 1–9 epoxide and 1–8 hydroxyl units adsorbed on a 6 × 6 lateral unit cell of graphene. As an example, we show the optimized atomic structures with the 9 epoxide and 8 hydroxyl groups in Fig. 5a and b, respectively, in which the functional groups are present on the both sides of graphene. This two-side adsorption is identified to be energetically favourable against the one-side configurations because of a cancellation of vertical structural distortion (Fig. S5†), as addressed in the previous studies.[36,37] The three distinct principal adsorption sites of epoxide and hydroxyl groups on graphene have been taken into account; namely hollow-, bridge-, and top-site. As shown in Fig. S1 and S2,† the total energy calculations show that the most stable adsorption site of the epoxide group is the bridge-site, whereas it is the top-site with C–O bond for the hydroxyl group. Overall the optimized atomic structures of graphene with the epoxide and hydroxyl species are in agreement with those reported in the previous studies.[36–38]

The oxide functional coverage of graphene surface can possibly exist in various configurations of the distribution. Among the several geometries explored, the top and side views of two selected patterns, named as 'uniform' (left panel) and 'island' (right panel), are shown in Fig. 5a and b for the two-sided epoxide and hydroxyl groups, respectively. In the uniform configuration, the functional groups are distributed evenly with the similar distances from each other across the graphene surface. In the island configuration, the functional groups are aggregated rather in close proximity within the highly oxidized domain like distribution. In order to identify a ground-state phase of oxygen distribution, we formulate the binding energetics (E_b) as[39]

$$E_b = \frac{E_{tot}(\text{graphene oxide}) - E_{tot}(\text{graphene}) - \sum_i N_i\mu_i}{N_i}, \quad (1)$$

where, E_{tot}(graphene oxide) and E_{tot}(graphene) are the total energies of graphene with the epoxide or hydroxyl functions and the pristine graphene, respectively. N_i is the number of atoms in the epoxide or hydroxyl groups, μ_i is the chemical potential of the i-th atomic species, *i.e.*, O and H, which is taken as the total energy of an isolated O (H) atom in a vacuum. According to eqn (1), E_b is then defined as change in energy when GO is formed from its constituents (*i.e.*, graphene and functional groups) in their reference states,[40] where the larger negative E_b implies the more favourable formation of the functional groups on graphene. As indicated in Fig. 5a and b, the calculated E_b are −2.52 and −3.18 eV per oxygen for the uniform and island phases of the 9-unit epoxide groups on graphene, respectively. Those for the 8-unit hydroxyl groups are −2.98 and −3.41 eV per oxygen, respectively. These results clearly indicate that both the epoxide and hydroxyl groups tend to adsorb on graphene in close proximity with domain like distribution rather than uniform one, in consistent with the present experiments (Fig. 2). It is also expected from our calculations that the presence of epoxide–hydroxyl pairs on graphene is most likely to be favoured over individual epoxide units, owing to the stronger binding affinity of hydroxyl/graphene sample, in consistent with the XPS data in the present experiments (epoxide and hydroxyl species are always coexisted, see Fig. 3) and previous calculations.[37] The further investigations demonstrate that this argument should also be applicable to the different coverages of the functional groups. As shown in Fig. 5c and d, the E_b decreases with the number of functional species for both the island epoxide and hydroxyl groups. As a generic, the saturation behaviour of E_b is well evident at the eight functional groups. For each functional group, we also compare the E_b between the one- (square) and two-sided (circle symbol) configurations in Fig. 5c and d, which reproduces the previous calculations for the better stability of the two-sided functional groups adsorbed onto the graphene surface.[36–38] The more detailed atomic structures of the different adsorption configurations and binding affinity calculations are provided in Fig. S1–S5 in the ESI† for the one- and two-sided 1 and 2 functional groups.

Next, the AIMD simulations are used to investigate the decomposition process of the functional groups from GO surface at an elevated temperature. As a precursor, only the two neighbouring epoxide-only and hydroxyl-only species, incorporating the energetically favourable building blocks,[41] chemisorbed onto the one-side of graphene have been modelled in the present computation. The left panels shown in Fig. 6a and b are the top and side views of the optimized atomic structures for the epoxide and hydroxyl groups on graphene at absolute

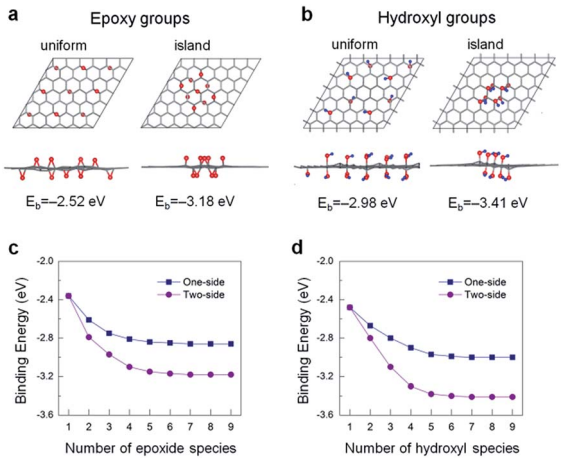

Fig. 5 Top and side views of the optimized atomic structures for uniform- and island-type distribution of (a) 9-unit epoxy groups and (b) 8-unit hydroxyl groups. The corresponding binding energies E_b of these groups are shown at the bottom of each panel. Red and blue spheres denote the oxygen and hydrogen atoms, respectively. E_b *versus* the number of (c) epoxide and (d) hydroxyl species for two configurations.

zero temperature, 0 K or −273.15 °C. It is seen that the presence of the functional groups can induce a tenuous local distortion in graphene lattice. This effect is indeed expected from the previous studies that the chemisorption of functional atoms (*e.g.*, O, H, and F) onto graphene results in a phase transition from planar sp^2 to distorted sp^3 like hybridization.[36–39,41] As temperature increases up to 300 °C, such a structural instability of graphene upon functionalization is even further deformed while the entire area of a flat graphene is significantly wrinkled, as seen in the middle and right panels in Fig. 6a and b. Furthermore, the C–O bond lengths of epoxide groups on graphene increase from about 1.44 Å at 0 K to 1.51 Å at 150 °C to 1.64 Å at 300 °C. This reveals a tendency of the functional group desorption from the graphene surface at high temperature although not complete.

Notably, the hydroxyl groups decompose into single oxygen atoms as an epoxide on graphene and desorbed water molecules (H_2O) even at 150 °C, where the GO surface would be served as a catalytic activity at finite temperature. We also show the temperature (both begin and end points at 150 °C) and total energy profiles during the AIMD simulation with 1000 ionic steps in Fig. 6c and d, respectively. The decomposition process from hydroxyl groups into H_2O molecules is also illustrated in the inset in Fig. 6d. The hydroxyl groups are first detached from graphene, and then the isolated water and oxygen atoms form. Such an oxygen atom eventually adsorbs onto graphene, making epoxide with graphene shown in the middle panel in Fig. 6b. We finally would like to note that the direct comparison between experimental and theoretical results requires some cautions, and the further simulations with more realistic geometric patterns – considering a broad ranges of sample stoichiometry with the presence of graphene defects (*e.g.*, edge and vacancy sites), different relative amounts and mixed phases of epoxide and hydroxyl groups, domains of various intermediate phases – should be carried out to provide more practical results and insights.

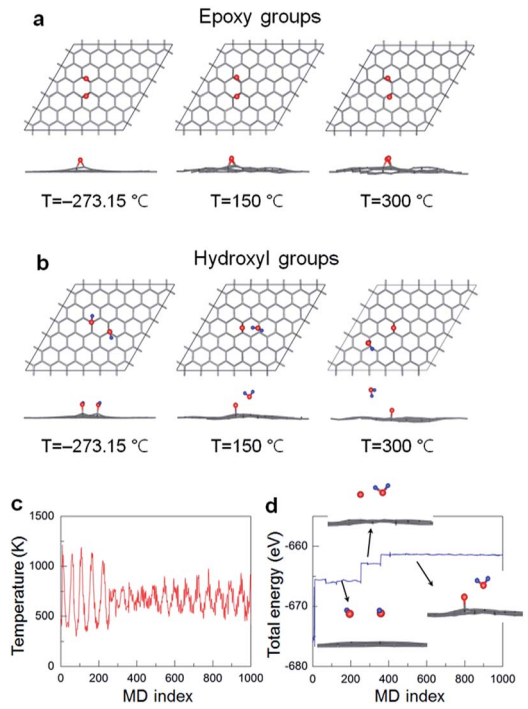

Fig. 6 AIMD simulations for the decomposition process of (a) epoxy groups and (b) hydroxyl groups at various temperatures. Atomic symbols are the same as used in Fig. 5. (c) Temperature and (d) energy profiles during AIMD simulation with 1000 ionic steps.

Conclusions

In summary, the oxygen functional groups on GOs treated at 150, 200, 250, and 300 °C was identified by the deposition of TiO_2 on the GO surface using ALD. We found that the oxygen functional groups are not distributed evenly but in the form of island. This structural information was obtained from the aberration corrected TEM and XPS. To understand this distribution of oxygen functional groups, we conduct the DFT calculations, where the binding energetics reveals that the oxygen functional groups prefer the island formation rather than uniform distribution. Moreover, the reduction process of epoxide and hydroxyl groups on GO surface at different temperatures was investigated with the ab initio molecular dynamics simulations. This work provides not only the fundamental properties of GO but also offers the information on designing the GO-based energy materials.

Acknowledgements

This work was supported by the Incheon National University Research Grant in 20141308. This work was also partially supported by the National University of Mongolia for the visiting fellowship research program (Grant No. P2016-1161).

References

1 S. Stankovich, D. A. Dikin, R. D. Piner, K. A. Kohlhaas, A. Klennhammes, Y. Jia, Y. Wu, S. T. Nguyen and R. S. Ruoff, *Carbon*, 2007, **45**, 1558–1565.
2 G. Hu, C. Xu, Z. Sun, S. Wang, H.-M. Cheng, F. Li and W. Ren, *Adv. Mater.*, 2016, **28**, 1603–1609.
3 J. Song, Z. Yu, M. L. Gordin and D. Wang, *Nano Lett.*, 2016, **16**, 864–870.
4 Y. Gong, S. Yang, Z. Liu, L. Ma, R. Vajtai and P. M. Ajayan, *Adv. Mater.*, 2013, **25**, 3979–3984.
5 S. I. Shin, A. Go, I. Y. Kim, J. M. Lee, Y. Lee and S.-J. Hwang, *Energy Environ. Sci.*, 2013, **6**, 608–617.
6 R.-Z. Li, R. Peng, D. D. Kihm, S. Bai, D. Bridges, U. Tumuluri, Z. Wu, T. Zhang, G. Compagnini, Z. Feng and A. Hu, *Energy Environ. Sci.*, 2016, **9**, 1458–1467.
7 C. Zhang, X. Wang, Q. Liang, X. Liu, Q. Weng, J. Liu, Y. Yang, Z. Dai, K. Ding, Y. Bando, J. Tang and D. Golberg, *Nano Lett.*, 2016, **16**, 2054–2060.
8 B. H. Kim, W. G. Hong, H. Y. Yu, Y.-K. Han, S. M. Lee, S. J. Chang, H. R. Moon, Y. Jun and H. J. Kim, *Phys. Chem. Chem. Phys.*, 2012, **14**, 1480–1484.

9 W. G. Hong, B. H. Kim, S. M. Lee, H. Y. Yu, Y. J. Yun, Y. Jun, J. B. Lee and H. J. Kim, *Int. J. Hydrogen Energy*, 2012, **37**, 7594–7599.
10 B. H. Kim, W. G. Hong, H. R. Moon, S. M. Lee, J. M. Kim, S. Kang, Y. Jun and H. J. Kim, *Int. J. Hydrogen Energy*, 2012, **37**, 14217–14222.
11 S. Liu, L. Sun, F. Xu, J. Zhang, C. Jiao, F. Li, Z. Li, S. Wang, Z. Wang, X. Jiang, H. Zhou, L. Yang and C. Schick, *Energy Environ. Sci.*, 2013, **6**, 818–823.
12 J. Liu, M. Durstock and L. Dai, *Energy Environ. Sci.*, 2014, **7**, 1297–1306.
13 M. Kotal, J. Kim, K. J. Kim and I.-K. Oh, *Adv. Mater.*, 2016, **28**, 1610–1615.
14 C. Li, L. Qiu, B. Zhang, D. Li and C.-Y. Liu, *Adv. Mater.*, 2016, **28**, 1510–1516.
15 D. Chen, H. Feng and J. Li, *Chem. Rev.*, 2012, **112**, 6027–6053.
16 C. Huang, C. Li and G. Shi, *Energy Environ. Sci.*, 2012, **5**, 8848–8868.
17 D. A. Dikin, S. Stankovich, E. J. Zimney, R. D. Piner, G. H. B. Dommett, G. Evmenenko, S. T. Nguyen and R. S. Ruoff, *Nature*, 2007, **448**, 457–460.
18 W. Gao, L. B. Alemany, L. Ci and P. M. Ajayan, *Nat. Chem.*, 2009, **1**, 403–408.
19 A. Y. S. Eng, C. K. Chua and M. Pumera, *Nanoscale*, 2015, **7**, 20256–20266.
20 A. Hunt, D. A. Kikin, E. Z. Kumaev, T. D. Boyko, P. Bazylewski, G. S. Chang and A. Moewes, *Adv. Mater.*, 2012, **22**, 3950–3957.
21 L.-C. Lin and J. C. Grossman, *Nat. Commun.*, 2015, **6**, 8335.
22 C. Gómez-Navarro, J. C. Meyer, R. S. Sundaram, A. Chuvilin, S. Kurasch, M. Burghard, K. Kern and U. Kaiser, *Nano Lett.*, 2010, **10**, 1144–1148.
23 K. Erickson, R. Emi, Z. Lee, N. Alem, W. Gannett and A. Zettl, *Adv. Mater.*, 2010, **22**, 4467–4472.
24 C. B. Boothroyd, M. S. Moreno, M. Duchamp, A. Kovacs, G. M. Morales, C. A. Barbero and R. E. Bunin-Borkowski, *Ultramicroscopy*, 2014, **145**, 66–73.
25 J. M. Kim, W. G. Hong, S. M. Lee, S. J. Chang, Y. Jun, B. H. Kim and H. J. Kim, *Int. J. Hydrogen Energy*, 2014, **39**, 3799–3804.
26 X. Gao, J. Jang and S. Nagase, *J. Phys. Chem. C*, 2010, **114**, 832–842.
27 C.-M. Chen, Q. Zhang, M.-G. Yang, C.-H. Huang, Y.-G. Yang and M.-Z. Wang, *Carbon*, 2012, **50**, 3572–3584.
28 S. Y. Lee, C. Jeon, S. H. Kim, Y. Kim, W. Jung, K. S. An and C. Y. Park, *J. Appl. Phys.*, 2012, **51**, 2–4.
29 D. M. King, X. Liang, Y. Zhou, C. S. Carney, L. F. Hakim, P. Li and A. W. Weimer, *Powder Technol.*, 2008, **183**, 356–363.
30 J. H. Yoon, S. C. Jung and J. S. Kim, *Mater. Chem. Phys.*, 2011, **125**, 342–346.
31 J. Lee, J. Yoon, H. G. Kim, S. Kang, W.-S. Oh, H. Algadi, S. Al-Sayari, B. Shong, S.-H. Kim, H. Kim, T. Lee and H.-B.-R. Lee, *NPG Asia Mater.*, 2016, **8**, e331.
32 P. E. Blochl, *Phys. Rev. B: Condens. Matter Mater. Phys.*, 1994, **50**, 17953.
33 G. Kresse and J. Hafner, *Phys. Rev. B: Condens. Matter Mater. Phys.*, 1993, **47**, 558.
34 J. P. Perdew, K. Burke and M. Ernzerhof, *Phys. Rev. Lett.*, 1996, **77**, 3865.
35 D. M. Bylander and L. Kleinman, *Phys. Rev. B: Condens. Matter Mater. Phys.*, 1992, **46**, 13756.
36 D. W. Boukhvalov and M. I. Katsnelson, *J. Am. Chem. Soc.*, 2008, **130**, 10697.
37 J. A. Yan, L. Xian and M. Y. Chou, *Phys. Rev. Lett.*, 2009, **103**, 086802.
38 J.-L. Li, K. N. Kudin, M. J. McAllister, R. K. Prudhomme, I. A. Aksay and R. Car, *Phys. Rev. Lett.*, 2006, **96**, 176101.
39 D. Odkhuu, D. Shin, R. S. Ruoff and N. Park, *Scientific Reports*, 2013, **3**, 3276.
40 D. Odkhuu, *Phys. Rev. B*, 2016, **94**, 060403.
41 S. S. Han, H. Jung, D. H. Jung, S. H. Choi and N. Park, *Phys. Rev. B: Condens. Matter Mater. Phys.*, 2012, **85**, 155408.